Small-Signal Modeling of Power Electronic Converters with Resonant Controllers

Peter W. Lehn, Stephen Podrucky

***Abstract*--While time domain electromagnetic transient simulation is an incredibly powerful tool for the analysis of large signal events in power systems, many small-signal phenomena may alternatively be studied using eigenvalue analysis and/or transfer functions. Eigenvalue or transfer function based analysis requires system linearization to be carried out about a static operating point. In the case of power systems, where voltage and current signals are AC, linearization is made possible through use of the synchronous or *dq* reference frame transformation. Since machine models and models of most FACTS devices and their controllers are readily available in the *dq*-frame, the process of linearizing such equipment is relatively straight-forward.**

Recently, resonant controllers have emerged as an alternative to *dq*-frame controllers for regulation of grid connected converters, both in FACTS devices and in interface converters for distributed resources. Although these control systems behave somewhat similar to *dq*-frame controllers under balanced operating conditions, their behaviour under unbalanced operation is unique.

This paper develops a small signal model of a VSC system, where resonant current controllers are used for regulation of the grid currents. Dynamics of a DC voltage control loop are included. Small signal dynamics are validated against time domain simulation.

***Keywords*: resonant control, FACTS, HVDC, active rectifier, eigenvalues, small signal analysis, converters, VSC.**

I. INTRODUCTION

WHEN attempting to regulate grid connected AC to DC converters, such as FACTS devices, *dq*-frame controllers are a standard approach [1]. Under balanced grid voltage operating conditions the *dq*-frame control strategy is a simple and effective solution. Recently, αβ-frame resonant controllers have emerged to serve in the place of *dq*-frame controllers [2], [3]. The primary difference between *dq*-frame and αβ-frame controllers is that the αβ-frame resonant controllers are able to track both balanced and unbalanced current reference commands [4]. However, one drawback of the αβ-frame current control is the appearance of time-invariant modulation blocks in its control loop. With the appearance of such time-invariant terms, control design and parameterization techniques such as eigenvalue analysis cannot be performed. Similar linearization techniques of a time-invariant system for VSC based HVDC transmission control is utilized in [5].

This paper will develop a linearization technique applicable to VSCs with αβ-frame controllers, thus making small signal system modeling possible. Validation of the new system model is carried out by comparing the linearized small signal model with large signal simulation results obtained from MATLAB/SIMULINK.

II. TYPICAL VSC CONTROL STRUCTURE

The electrical diagram of a VSC based AC to DC controller is shown in Fig. 1. The discussion of this paper is with respect to this 3-phase AC to DC converter, which may be used as a building block to develop more elaborate FACTS controllers, VSC based HVDC systems or as part of an electrical drive system.

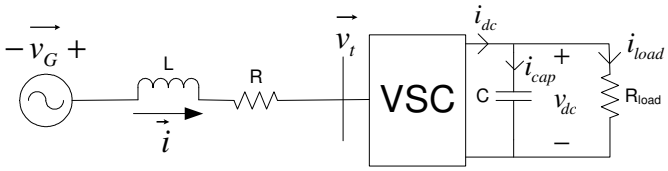

Fig.1. Single line diagram for series voltage sourced converter

Based on time-averaging assumptions, Fig. 2 provides a large-signal αβ-frame model of the converter dynamics, useful for computationally efficient time-domain simulation. The inner αβ-frame current control loop, given in Fig.4, contains a resonant controller for both the α and β-axis currents. Under unbalanced operating conditions, this controller can (i) reject unbalanced grid voltage distortions and (ii) track unbalanced current references, if desired. This eliminates not only the need for separate controllers for positive and negative sequence components, but also eliminates the filtering required to separate the positive from negative sequence components, as discussed in [4].

Only two blocks in the diagram of Fig. 2 are not linear time-invariant. One of these blocks appears after the DC voltage controller. It is a modulator used to create the required αβ-frame current references. The other is the AC to DC power conversion equation, which relates the converter's dc-side voltage and current to its ac-side voltage and current in the αβ-frame. Embedded in this power equation is a demodulation function.

In Fig.3, the demodulating function and the power equation have been separated. The extraction of the demodulating element transfers the αβ-frame power conversion equation into the *dq*-frame. Neither the demodulation function, nor the power equation are linear time-invariant.

This work was funded by the Natural Science and Engineering Research Council of Canada

P.W. Lehn and S. Podrucky are with the Department of Electrical and Computer Engineering, University of Toronto, Toronto, Ontario, Canada, M5S 3G4 (e-mail: lehn@ecf.utoronto.ca, stephen.podrucky@utoronto.ca)

Paper submitted to the International Conference on Power Systems Transients (IPST2009) in Kyoto, Japan June 3-6, 2009

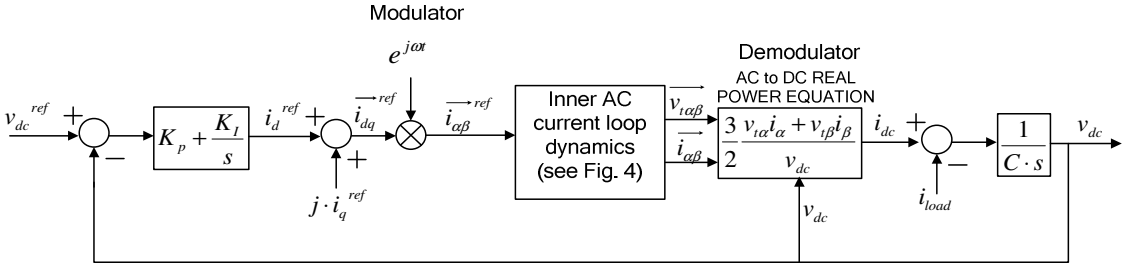

Fig. 2. Block diagram of DC voltage control model with αβ frame current control

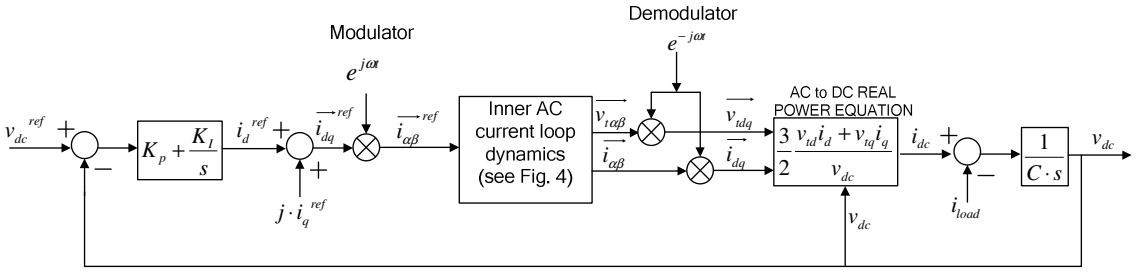

Fig. 3. Block diagram of DC voltage control model with αβ frame current control modified

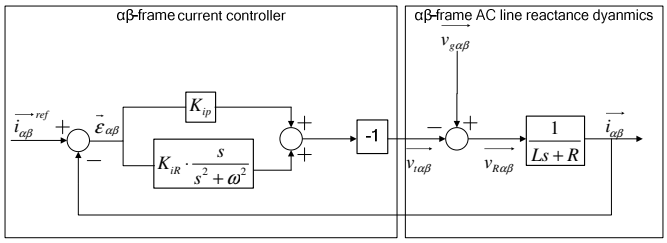

Fig. 4. Inner AC current loop of Fig.2

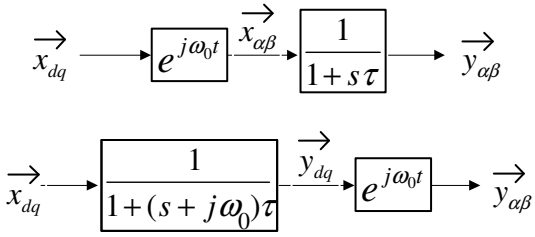

Fig.5. Shifting of rotating space vector

To allow use of linear analysis (e.g. eigenvalue analysis) and control design techniques (e.g. root locus, bode plot or linear state space control techniques) the structure of Fig. 2 must be linearized. This is achieved by manipulation of the equivalent system shown in Fig. 3. The process, will create a *dq*-frame equivalent of the αβ-frame current controller. Unlike the original αβ-frame model the *dq*-frame equivalent will:

(i) contain only time-invariant blocks

(ii) be linearizable about a nominal operating point.

III. DQ-FRAME EQUIVALENT OF ALPHA BETA-FRAME RESONANT CURRENT CONTROLLER

Utilizing the block diagram based reference frame transformation approach of [6], the $e^{j\omega t}$ term can be moved through the αβ current controller. The transformation approach is depicted in Fig. 5, where the transfer function parameter τ may, in general, be complex.

By performing this shift through a transfer function, each pole and zero of the transfer function is shifted by $j\omega_0$. The resulting shifts in each αβ-frame transfer function can be viewed in Table I. These results are in agreement with those of Zmood, Holmes, and Bode [7].

TABLE I
TRANSFORMATION OF ALPHA-BETA FRAME CURRENT CONTROLLER

αβ Frame Transfer Function	Equivalent dq-frame Transfer Function
K_{ip}	K_{ip}
$K_{iR}\cdot\frac{s}{s^2+\omega^2}$	$K_{iR}\cdot\frac{(s+j\omega)}{s(s+j2\omega)}$ $= K_{iR}\cdot\left[\frac{(s^2+2\omega^2)}{s(s^2+4\omega^2)} - j\cdot\frac{\omega}{s^2+4\omega^2}\right]$ $= C_{\mathrm{Re}}(s) - j\cdot C_{\mathrm{Im}}(s)$

Using results from Table I, the block diagram of Fig. 6 may be constructed using the relations:

$$\vec{v}_{dq} = (C_{\mathrm{R}}(s) - jC_{\mathrm{I}}(s))(\varepsilon_d + j\varepsilon_q) \quad (1)$$

$$\vec{v}_{dq} = (\varepsilon_d C_{\mathrm{R}} + \varepsilon_q C_{\mathrm{I}}) + j(\varepsilon_q C_{\mathrm{R}} - \varepsilon_d C_{\mathrm{I}}) \quad (2)$$

where K_{ip} is the proportional current control gain, K_{ir} is the resonant current control gain, ε_d is the error of the d-axis current control, ε_q is the error of the q-axis current control.

From the *dq*-frame equivalent block diagram of Fig.6, one can note a change in structure. While the grid voltage and the AC plant dynamics are simply replaced by their *dq*-frame equivalents, the current controller contains cross coupling transfer functions between the d and q-axes.

IV. Small Signal Modeling and Linearization about Balanced Source Operating Point

Having shifted the $e^{j\omega t}$ modulator rightwards through the current loop allows the modulator/demodulator functions to be cancelled. As can be observed in Fig. 6 the resulting current loop is now in the *dq*-frame. Combining the DC voltage control loop of Fig. 3 with the current control loop of Fig. 6 yields a complete, large-signal, *dq*-frame model, as shown in Fig. 7. Fig. 2 and Fig. 7 are therefore equivalent and may be interchangeably used for large-signal simulation (based on time averaging assumptions).

The only non-linearity in Fig. 7 resides in the AC to DC power conversion equation. This function can be easily linearized using small-signal conversion of a non-linear system. Similar techniques are utilized in DC to DC converters, [9]. A Taylor series was applied to the non-linear power equation (3) to obtain our linear model (4). The time varying small signal variables in (4) are denoted with an inflection above them. Capital variables stand for the steady state operating point values of the given system.

$$i_{dc} = \frac{3}{2} \cdot \frac{v_{td} i_d + v_{tq} i_q}{v_{dc}} \tag{3}$$

$$\hat{i}_{dc} = \frac{3}{2 \cdot V_{dc}} [\hat{v}_{td} I_d + \hat{v}_{tq} I_q + \hat{i}_d V_{td} + \hat{i}_q V_{tq}] - \frac{I_{dc}}{V_{dc}} \cdot \hat{v}_{dc} \tag{4}$$

where v_{td} is the d-axis VSC AC side terminal voltage, v_{tq} is the q-axis VSC AC side terminal voltage, i_d is the d-axis AC line current, i_q is the q-axis AC line current, v_{dc} is the DC link voltage of the VSC, and i_{dc} is the current from the VSC into the DC link.

Now that each element of this *dq*-frame equivalent to the αβ current controller is linear, controller design techniques and linear analysis techniques, including eigenvalue analysis and system parameterization, can be performed. For these techniques to be easily implemented the state space representation of the closed loop system was developed and can be viewed in the Appendix. The small signal state space representation in the Appendix takes on the form of (5) and (6).

$$\frac{d\hat{x}}{dt} = A\hat{x} + B\hat{u} \tag{5}$$

$$\hat{y} = C\hat{x} \tag{6}$$

$$\hat{x} = [\hat{x}_{dc} \quad \hat{x}_{d1} \quad \hat{x}_{d2} \quad \hat{x}_{d3} \quad \hat{x}_{q1} \quad \hat{x}_{q2} \quad \hat{x}_{q3} \quad \hat{i}_d \quad \hat{i}_q \quad \hat{v}_{dc}]^T \tag{7}$$

Where $\hat{x}$ is the vector of small signal system variables, $\hat{u}$ the system inputs and $\hat{y}$ the system outputs.

With respect to (7), the first state variable is related to the DC voltage controller. The following two groups of three are linearly independent states that represent the states of the d and q axis current controllers. The next three states are the system's output states. With the linearized state space representation, a time domain simulation can be easily performed and the small signal model of the control system can be validated.

V. Model Validation via Time Domain Simulations

The performance of the small signal model for the DC voltage controller was tested against time domain simulation using MATLAB/SIMULINK. The response of the two system models were compared by viewing the DC link voltage, the *d*-axis AC line current, and the *q*-axis AC line current with respect to two input step changes:

(i) a +2A (0.17p.u.) step in DC load current

(ii) a +25V (0.067p.u.) step in the DC voltage reference.

The system parameters and steady state operating point values can be viewed in Table II below. Parameters for a low power 4.5 kVA VSC are used to allow future laboratory validation.

TABLE II
PARAMETERS USED IN SIMULATION

System Parameters	**Variable/Symbol**	**Value**
Grid voltage	Vg	208 V_{ll}
Converter Parameters	**Variable/Symbol**	**Value**
AC interface inductance	L	2.5 mH
AC interface resistance	R	0.52 Ω
DC link capacitor	C	70 μF
Converter Ratings		
kVA rating	Sbase	4.5 kVA
AC voltage rating	Vbase	120 V_{ln}
AC current rating	Ibase	12.5 A
DC voltage rating	Vdc_rated	375 V
Steady State Operating Conditions	**Variable/Symbol**	**Value**
D-axis grid voltage	Vgd	169.7 V
Q-axis grid voltage	Vgq	0 V
D-axis terminal voltage	Vtd	161.66 V
Q-axis terminal voltage	Vtq	-14.57 V
D-axis AC line current	Id	15.46 A
Q-axis AC line current	Iq	0 A
DC link current	Idc	10 A
DC link voltage	Vdc	375 V

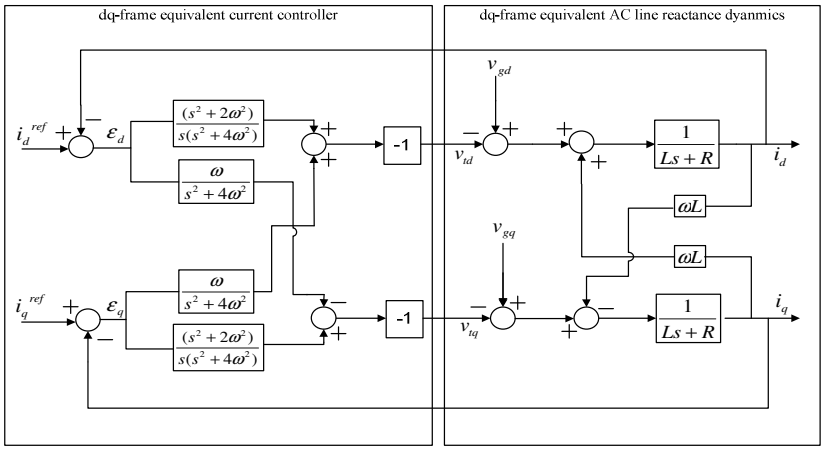

Fig.6. Dq-frame equivalent of αβ-frame current loop of Fig.4

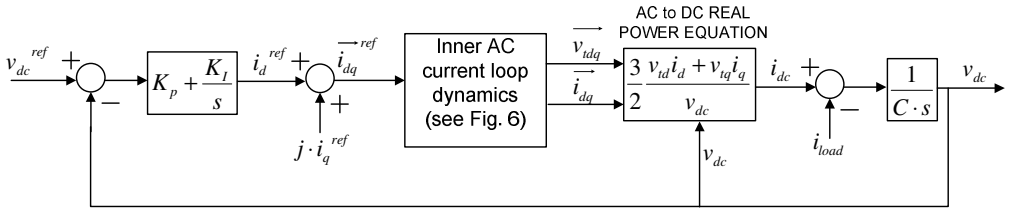

Fig. 7. Dq-frame block diagram equivalent of Fig. 2.

A. DC Load Current Step Response

The converter is first operated as an active rectifier and a step change in DC load current is introduced to the system. At time 1 second the DC load current is increased from 10 A to 12 A. The responses of large and small signal systems are compared in Fig 8.

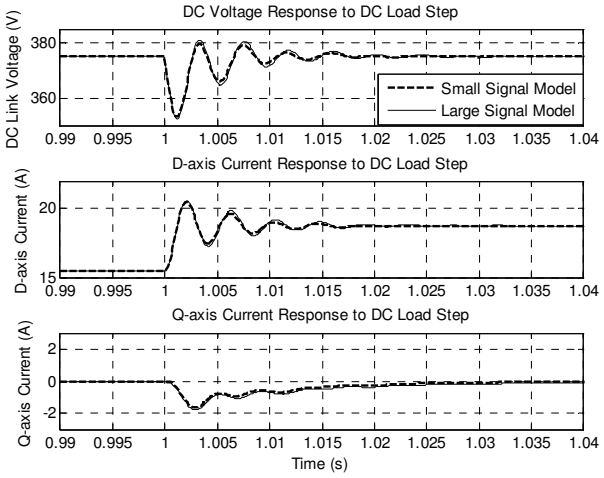

Fig. 8 Responses to DC load step change

From viewing Fig. 8 one can note very little deviation between the large and small signal system responses as a result of a DC load step.

B. DC Link Voltage Reference Step Response

A change in DC link voltage reference is made to the simulated systems at time 1 second, with the DC voltage reference being increased from 375 to 400 V. The responses of the large and small signal systems are given in Fig. 9.

From viewing Fig. 9, one can again note very little deviation between the large and small signal system responses. The simulation results of Fig. 8 and 9 validate the accuracy of the developed small signal model.

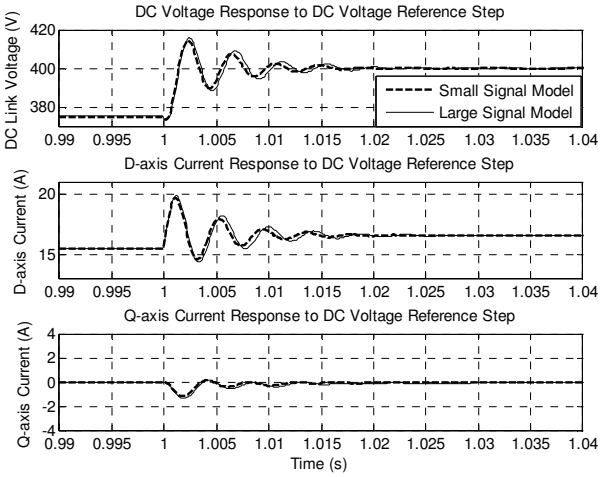

Fig. 9 Responses to DC voltage reference step change

VI. APPLICATIONS

Small signal converter models have many applications ranging from stability analysis to control design. In power systems, one application is to employ the small signal model to investigate the system dynamics after a fault event. In contrast to large signal simulation models, a small signal model allows

the dynamics to be related back to system and control parameter values.

In contrast, developers of electric drives, VSC based HVDC systems or wind turbine systems with back-to-back converter interface, designers may instead be interested in the DC-side input/output impedance of a converter, as this impedance may be used for investigating DC side interactions.

Two applications will be presented. The first investigates the small signal dynamics of a VSC interfaced energy source, where the AC grid is subjected to a distant line-line fault or distant 3-phase fault. The second application investigates the DC-side output impedance of the VSC when it is operated as a unity power factor active rectifier.

A. Converter Dynamics due to Distant Grid Faults

Two types of distant grid faults will be considered, namely a 3-phase fault and a line-line fault. Grid voltages before, during and after the fault are summarized in the table below.

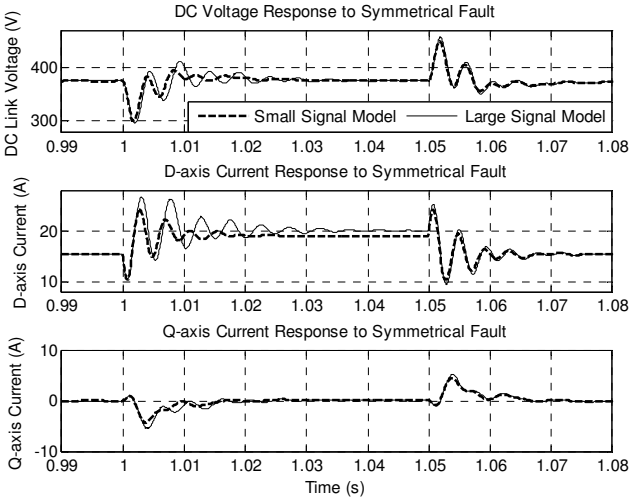

Fig. 10 Small signal converter response to a distant 3-phase fault.

TABLE III
LOCAL GRID VOLTAGE VARIATION DUE TO FAULT

	Va Phasor	Vb Phasor	Vc Phasor
Balance Fault			
Pre-fault	120∠0°	120∠120°	120∠240°
Fault	96∠0°	96∠240°	96∠240°
Post-fault	120∠0°	120∠120°	120∠240°
Unbalanced Fault			
Pre-fault	120∠0°	120∠120°	120∠240°
Fault	120∠0°	105.4∠124.7°	105.4∠235.3°
Post-fault	120∠0°	120∠120°	120∠240°

The response to a balanced distant fault is shown in Fig. 10. During the 3-phase fault a significant dip in grid voltage introduces some inaccuracy in the linearized model behavior. However, when the fault is cleared the recovery dynamics of the linearized system are highly accurate. The response to a line-line distant fault is shown in Fig. 11. Three traces are shown in Fig. 11; the linearized system behavior of the VSC with resonant control, the large signal behavior of the VSC with resonant control and the large signal behavior of a classical *dq*-frame controller. We can make three key observations:

1. Despite αβ-frame and *dq*-frame controllers being used almost interchangeably in the literature, a large difference exists in their response to unbalanced events.
2. Despite the ability of the resonant current control loop to reject any grid voltage imbalance, unbalanced currents still flow in the system, due to control action of the DC voltage regulator.
3. The linearized model accurately captures the dynamics associated with the unbalanced fault.

B. Converter DC-Side Output Impedance when Operated as a Unity Power Factor Active Rectifier

When inter-connecting multiple converters, as is done in back-to-back HVDC systems, electric drives and cascaded power supply systems, the circle criterion is sometimes used to determine stability of the inter-connected system, [10].

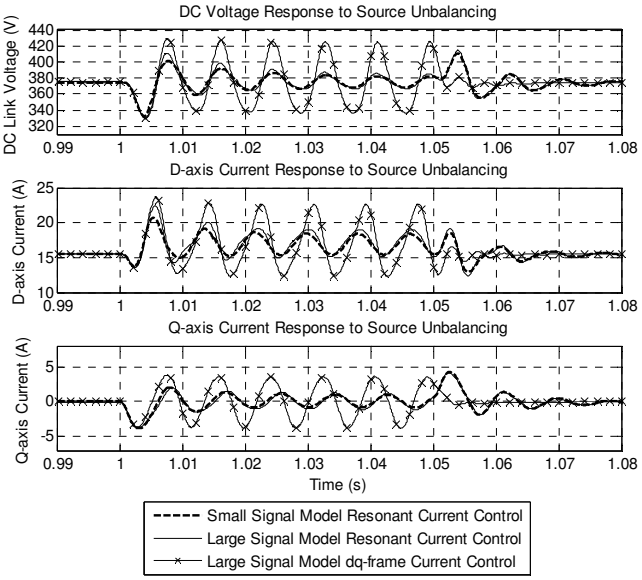

Fig. 11 Converter response to a distant line-line fault.

Application of the circle criterion requires the output (or input) impedance of each converter to be known. When operating as a unity power factor active rectifier, the transfer function from i_{load} to v_{dc} (see Fig.1) gives the dc-side output impedance of the converter. This may be found from the linearized model from:

$$Z(s) = \frac{V_{dc}(s)}{I_{dc}(s)} = C_m(sI - A)^{-1}B_m \qquad (7)$$

where $A = \begin{bmatrix} A_1 & A_2 \\ A_3 & A_4 \end{bmatrix}$ with sub-matrices given in the appendix, C_m= [0 0 0 0 0 0 0 0 0 1], and B_m = [0 0 0 0 0 0 0 0 0 -1/C]^T.

Fig. 12 and Fig. 13 show the magnitude and angle of the DC-side output impedance. Using successive time domain simulations, the small signal impedance is verified at five discrete frequencies, as shown by the 'x' markers in Fig. 12. The linearized results again show excellent accuracy up to several hundred hertz.

VII. CONCLUSIONS

A complete small signal model of the VSC with αβ-frame control is developed and validated. Since linearization of the system must be carried out around a sinusoidal operating point, the αβ-frame control and system models must be first converted into equivalent *dq*-frame control and system models. The conversion is carried out using a simple block diagram manipulation approach. The resulting *dq*-frame model is finally linearized. The resulting state space matrix equations is developed parametrically so that users may explore the effects of controller gains, parameter values and operating point on the system dynamics.

The developed model has been validated against time domain simulation results. Two applications of the model, one to power system dynamics and the other to motor drive/HVDC system stability analysis give brief examples of how the model might be used.

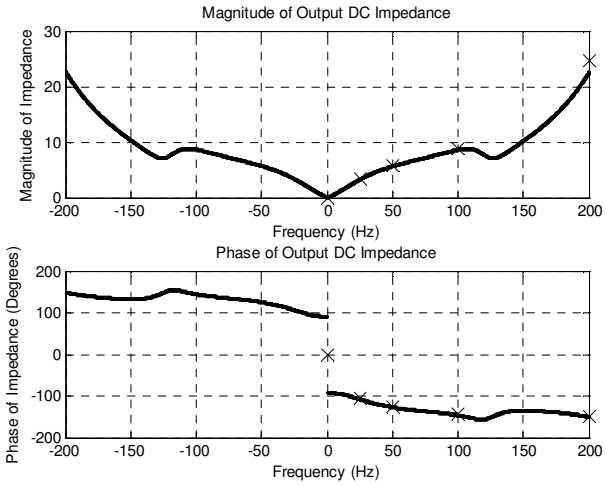

Fig. 12 Magnitude and phase of output DC impedance

VIII. APPENDIX

$$\frac{d\hat{x}}{dt}=\begin{bmatrix}A_1 & A_2\\ A_3 & A_4\end{bmatrix}\hat{x}+\begin{bmatrix}K_I & 0 & 0 & 0 & 0\\ 0 & 0 & 0 & 0 & 0\\ 0 & 0 & 0 & 0 & 0\\ K_P & 0 & 0 & 0 & 0\\ 0 & 0 & 0 & 0 & 0\\ 0 & 0 & 0 & 0 & 0\\ 0 & 1 & 0 & 0 & 0\\ \frac{K_{iP}K_P}{L} & 0 & \frac{1}{L} & 0 & 0\\ 0 & \frac{K_{iP}}{L} & 0 & \frac{1}{L} & 0\\ \frac{-3K_{iP}K_PI_d}{2V_{dc}C} & \frac{-3K_{iP}I_q}{2V_{dc}C} & 0 & 0 & \frac{-1}{C}\end{bmatrix}\hat{u}$$

$$A_1=\begin{bmatrix}0 & 0 & 0 & 0 & 0\\ 0 & 0 & 1 & 0 & 0\\ 0 & 0 & 0 & 1 & 0\\ 1 & 0 & -4\omega^2 & 0 & 0\\ 0 & 0 & 0 & 0 & 0\end{bmatrix}\qquad A_2=\begin{bmatrix}0 & 0 & 0 & 0 & -K_I\\ 0 & 0 & 0 & 0 & 0\\ 0 & 0 & 0 & 0 & 0\\ 0 & 0 & 0 & -1 & -K_P\\ 1 & 0 & 0 & 0 & 0\end{bmatrix}$$

$$A_3=\begin{bmatrix}0 & 0 & 0 & 0 & 0\\ 0 & 0 & 0 & 0 & 0\\ \frac{K_{iP}}{L} & \frac{2K_{iR}\omega^2}{L} & 0 & \frac{K_{iR}}{L} & 0\\ 0 & 0 & \frac{-K_{iR}\omega}{L} & 0 & \frac{2K_{iR}\omega^2}{L}\\ \frac{-3K_{iP}I_d}{2V_{dc}C} & \frac{-3K_{iR}\omega^2I_d}{V_{dc}C} & \frac{3K_{iR}\omega I_q}{2V_{dc}C} & \frac{-3K_{iR}I_d}{2V_{dc}C} & \frac{-3K_{iR}\omega^2I_q}{V_{dc}C}\end{bmatrix}$$

$$A_4=\begin{bmatrix}0 & 1 & 0 & 0 & 0\\ -4\omega^2 & 0 & 0 & -1 & 0\\ \frac{K_{iR}\omega}{L} & 0 & \frac{-R}{L}-\frac{K_{iP}}{L} & \omega & \frac{-K_{iP}K_P}{L}\\ 0 & \frac{K_{iR}}{L} & -\omega & \frac{-R}{L}-\frac{K_{iP}}{L} & 0\\ \frac{-3K_{iR}\omega I_d}{2V_{dc}C} & \frac{-3K_{iR}I_q}{2V_{dc}C} & \frac{3(V_{td}+K_{iP}I_d)}{2V_{dc}C} & \frac{3(V_{tq}+K_{iP}I_q)}{2V_{dc}C} & \frac{3K_{iP}K_PI_d-2I_{dc}}{2V_{dc}C}\end{bmatrix}$$

$$\hat{y}=\begin{bmatrix}0 & 0 & 0 & 0 & 0 & 0 & 0 & 1 & 0 & 0\\ 0 & 0 & 0 & 0 & 0 & 0 & 0 & 0 & 1 & 0\\ 0 & 0 & 0 & 0 & 0 & 0 & 0 & 0 & 0 & 1\end{bmatrix}\cdot\hat{x}$$

$$\hat{u}=\begin{bmatrix}\hat{v}_{dc}^{\ ref} & \hat{i}_q^{\ ref} & \hat{v}_{gd} & \hat{v}_{gq} & \hat{i}_{load}\end{bmatrix}^T$$

IX. REFERENCES

[1] M. Cichowlas and M.P. Kamierkowski, "Comparison of current control techniques for PWM rectifiers," *IEEE International Symposium on Industrial Electronics*, Vol.4, November 2002, pp. 1259-1263.

[2] D.N. Zmood and D.G. Holmes, "Stationary frame current regulation of PWM inverters with zero steady-state error," *IEEE Trans. On Power Electronics*, Vol 18, May 2003, pp. 814-822.

[3] J.G. Hwang, M. Winkelnkemper, and P.W. Lehn, "Design of an Optimal Stationary Frame Controller for Grid Connected AC-DC Converters," *32nd Annual Conference on IEEE Industrial Electronics 2006*, Nov. 2006, pp. 167-172.

[4] J.G. Hwang, and P.W. Lehn, "DC space vector controller and its application to converter control," *P.E.S.C. 2008*, June 2008, pp. 830-836.

[5] D. Jovcic, L.A Lamont and L. Xu, " VSC transmission model for analytical studies," *IEEE Power Engineering Society General Meeting 2003*, Vol. 3, July 2003, pp. 1737-1742.

[6] C. Sao and P.W. Lehn, "A block diagram approach to reference frame transformation of converter dynamic models," *IEEE 18th Canadian Conf. Elec. And Comp. Eng., CCECE2006,* May 2006.

[7] D.N. Zmood, D.G. Holmes, and G.H. Bode, "Frequency-Domain Analysis of Three-Phase Linear Current Regulators," *IEEE Trans. on Ind. App.*, Vol. 37, April/March 2001, pp. 601-610.

[8] J.G. Hwang, P.W. Lehn, and M. Winkelnkemper, "Control of AC-DC-AC converters with minimized DC link capacitance under grid distortion," *2006 IEEE International Symposium on Industrial Electronics*, Vol. 2, July 2006, pp. 1217-1222.

[9] R. W. Erickson and D. Maksimović, *Fundamentals of Power Electronics*, 2nd ed., Springer Science+Business Media, LLC, 2001, pp. 197-221.

[10] M.Vidyasagar, *Nonlinear Systems Analysis*, 2nd ed., Prentice-Hall, 1993.